Agricultural and Forest Meteorology 226–227 (2016) 80–95

Contents lists available at ScienceDirect

Agricultural and Forest Meteorology

journal homepage: www.elsevier.com/locate/agrformet

Statistical analyses of potential evapotranspiration changes over the period 1930–2012 in the Nile River riparian countries

Charles Onyutha*

Faculty of Technoscience, Muni University, P.O. Box 725, Arua, Uganda

ARTICLE INFO

Article history:
Received 29 January 2016
Received in revised form 13 May 2016
Accepted 22 May 2016

Keywords:
CRD Test
Trend Analyses
NAIM
Variability Analyses
Nile River
Evapotranspiration

ABSTRACT

Changes in potential evapotranspiration (PET) in the Nile Basin tend to be analyzed mostly based on short-term remotely sensed annual data. In this study, long-term country-wide series from 1930 to 2012 were used to assess changes in annual and seasonal PET in all the Nile River Riparian Countries (NRRCs). Variability was investigated using the nonparametric anomaly indicator method. Trend was assessed both graphically and statistically using the cumulative rank difference method. The PET totals from 1930s to 1970s (from around 1980 to early 2000s) were generally below (above) the mean of the long-term data. Moreover, for this period from around 1980 to early 2000s, both annual and seasonal PET totals in most of the NRRCs were characterized by an increase significant at 5% level. This increase in the PET influenced the long-term trend based on the full time series from 1930 to 2012 towards positive direction. For instance, the long-term annual PET exhibited increasing trend significant at 5% level in 2 of the 6 countries in the equatorial region. However, the positive trends in the PET of Sudan, Ethiopia, Eritrea and Egypt were insignificant at 5% level. It was found that the temporal changes in PET especially during rainy seasons can be explained at the significance level of 5% by the rainfall variation. Sampling uncertainties on the PET trend magnitudes are quantified and provided. The findings in this study are important for determining the crop water requirements especially in arid conditions where rainfall is unreliable and low in volume.

1. Introduction

Analyses of the changes in potential evapotranspiration (PET) are vital to obtain acumen about the influence of land-atmosphere interactions and/or climate system on hydro- and agro-meteorology. The unswerving dependence of majority of the people within the Nile Basin on agriculture for their livelihoods (International Water Management Institute [IWMI], 2014), and the effect of climate variability on hydro-meteorological variables make food insecurity a formidable challenge that the Nile River Riparian Countries (NRRCs) have to deal with. One form of support in tackling such a challenge is a comprehensive study of the historical PET changes and the possible associated driving forces. Such support would be valuable for determining the crop water requirements especially in arid conditions where rainfall is unreliable and low in volume. Apart from the Ethiopian Highlands and the equatorial region which receive large amounts of rainfall annually, other parts of the study area experience both hyper-arid and sub-humid conditions.

Analyses of the changes in hydro-meteorological variables require long-term series of historical or observed data to minimize bias on the statistical results (Onyutha et al., 2015). However, due to the data limitation in the Nile Basin, the analyses of PET changes conducted in studies by e.g. Alemu et al. (2014), and Bashir et al. (2008) have been based on short-term remotely sensed data. For an insight into the temporal variability and long-term trends, it is vital to analyze changes in the PET based on rather long-term historical series than the remotely sensed data.

In this study, detection of changes in the long-term historical PET was two-fold. Firstly, long-term trend was assessed in terms of the significance of the non-zero slope of a linear variation of the PET with time. Secondly, variability was investigated in terms of the short-durational changes in the PET totals relative to the mean of the full time (long-term) series. Some of the nonparametric trend detection methods include the Mann-Kendall (MK) (Mann, 1945; Kendall, 1975), Spearman's rho (SMR) (Lehmann, 1975; Sneyers, 1990; Spearman, 1904), and the Cumulative Rank Difference (CRD) (Onyutha, 2016a) tests. These methods were demonstrated to perform comparably by Yue et al. (2002) for MK and SMR, and Onyutha (2016a) for MK and CRD. Thus, the CRD deemed to be representative for the analyses of PET trends was adopted in this study. On the other hand, some of the key methods

* Corresponding author.
E-mail address: conyutha@gmail.com

http://dx.doi.org/10.1016/j.agrformet.2016.05.015
0168-1923/

for computing variability include: (1) the autocorrelation spectral analysis (Blackman and Tukey, 1959; World Meteorological organization [WMO] 1966), and (2) empirical orthogonal functions. To assess variability in the PET, the Nonparametric Anomaly Indicator Method NAIM (Onyutha, 2016b), as will be presented in Section 3.1.3, was adopted in this study based on its suitability for non-normally distributed data and the robustness to deal with the influence of outliers in the series.

In statistical analyses of trends, a number of data related uncertainty sources exist some of which include: (1) data structure characterized by ties, serial correlation, etc which jointly invalidate the change-detection test assumption of the independence of observations; (2) data limitation in the form of short record length; and (3) data quality resulting from erroneous observations that can falsify the trend analyses results. In this study, the uncertainties on the trends are quantified by employing a technique herein coined as the Exclude-one and Estimate Slope (EES).

2. Study area and data

2.1. Study area

The study area (see Fig. 1) comprises the River Nile which is the world's longest river under arid condition and has a drainage area of about 3,400,000 km^2. The River Nile has two sources including the White Nile (from the equatorial region), and the Blue Nile (from the Ethiopian Highlands). About 50% of the River Nile flow is lost by evaporation in the Sudd region of South Sudan. The coverage of the NRRCs as a percentage of the total area of the Nile Basin (Food and Agriculture Organization [FAO], 1997) is: Uganda (7.4%), Kenya (1.5%), Tanzania (2.7%), Rwanda (0.6%), Burundi (0.4%), Democratic Republic of Congo (DRC) formerly known as Zaire (0.7%), Sudan (inclusive of the current South Sudan) (63.6%), Ethiopia (11.7%), Eritrea (0.8%), and Egypt (10.5%). The climate of the NRRCs is characterized by a strong latitudinal wetness gradient (Camberlin, 2009; Onyutha, 2016b). Whereas some parts of the study area such as the Ethiopian Highlands and Equatorial region receive annual rainfall in excess of 1000 mm, the areas which are not reached by the inter-tropical convergence zone (ITCZ) i.e. the northern most part of Sudan up to Egypt experience arid condition (Camberlin, 2009).

2.2. Data

Country-wide total monthly PET series (Harris et al., 2014) for the period 1930–2012 were obtained via the British Atmospheric Data Centre (BADC) (2014). Harris et al. (2014) computed the PET (mm/day) as a variant of the Penman-Monteith method using half degree gridded absolute values of mean temperature (°C), maximum temperature (°C), minimum temperature (°C), vapor pressure (hPa), cloud cover (%), and wind speed (m/s). The Penman-Monteith method was proposed by Food and Agriculture Organization as the standard method to calculate PET or Reference evapotranspiration (Allen et al., 1989). Long-term country-wide monthly rainfall data over the period 1930–2012 were also obtained from the same source as that for the PET i.e. (BADC, 2014; Harris et al., 2014). Rainfall data were obtained mainly for two reasons: firstly, to confirm whether the patterns of monthly rainfall totals in the study area are consistent with those known from past studies. Secondly, rainfall was also used to assess whether its variation can be used to explain the changes in PET. Because the series from the Climatic Research Unit (CRU) were already quality controlled (BADC, 2014), it was confirmed in this study that the data sets of both rainfall and PET had no missing values. Note should be taken that although South Sudan recently got independence from Sudan in 2011, the data under the name Sudan comprised averages over both Sudan and South Sudan.

Fig. 2 shows the monthly rainfall and PET patterns of all the NRRCs based on the data from 1930 to 2012. The rainfall pattern of the equatorial region (countries labeled (1) to (6) in Fig. 1) is bimodal and the "long-rains" and "short-rains" occur over the months of March–May (MAM) and October–December (OND) respectively (Nicholson, 1996). The long and short dry periods respectively occur over the months of June–September (JJAS) and January–February (JF) (Fig. 2a–f). The rainfall over the countries (7) to (9) is of a unimodal pattern with the JJAS (MAM) as the main (slight) rainy season (Camberlin, 2009), and October–February (ONDJF) the dry season (Fig. 2g–i). For Egypt, the long-term mean monthly rainfall is of more unclear patterns than for other countries (1–9); however, the wet (dry) season can be identified as MAM, ONDJF (JJAS). On the other hand, it is noticeable that Egypt's PET (Fig. 2j) is more distinctively of a unimodal pattern than that for the rest of the NRRCs (Fig. 2a–i). Fig. 2 suggests that the patterns of the monthly rainfall data obtained from Harris et al. (2014) and/or BADC (2014) are consistent with those from past studies. Because of the importance of rainfall seasonality for agriculture in the study area, the seasonal PET totals were computed based on the seasons of the rainfall (Fig. 2). However, annual time scale was also considered for the statistical assessment of changes in the PET.

3. Methodology

3.1. Cumulative rank difference (CRD) method

Although it was already mentioned in Section 1 that the CRD was adopted because it is comparable to both the SMR and MK in terms of performance, another reason for its use in this study also followed the fact that it employs both the statistical and graphical approaches for trend detection. Instead of testing for hydro-meteorological change in a purely statistical or mathematical way which can give meaningless results in some cases (Kundzewicz and Robson, 2000), graphical technique of exploratory data analyses is important to reveal hidden features such as sub-trends. The CRD method of change detection considers rescaling of the given time series of size n nonparametrically in terms of the difference d (Eq. (1)) between the exceedance and non-exceedance counts of data points.

$$d_i = u_i - v_i = 2u_i - (n - w_i) \text{ for } 1 \le i \le n \quad (1)$$

where u_i is the number of times the i^{th} data point is exceeded, v_i the number of times the i^{th} data point exceeds others, and w_i the number of times the i^{th} data point appears within the given sample. To determine u_i, v_i or w_i, each data point is counted as if it was not considered before (Onyutha, 2016b). For illustration, consider the hypothetical data set of $n = 10$ with data points 33, 14, 33, 29, 20, 33, 14, 27, 31, 50; the values of w_i and u_i at $i = 1, 2, \ldots, 10$ are (3, 2, 3, 1, 1, 3, 2, 1, 1, 1) and (1, 8, 1, 5, 7, 1, 8, 6, 4, 0) respectively. Correspondingly, the rescaled series d_i is (−5, 8, −5, 1, 5, −5, 8, 3, −1, −9). The cumulative sum (s_i) of the difference d_i in the ranks is obtained using Eq. (2).

$$s_i = \sum_{j=1}^{i} d_i \text{ for } 1 \le i \le n \quad (2)$$

For the above hypothetical series, the values of s_i would be (−5, 3, −2, −1, 4, −1, 7, 10, 9, 0). Because $\sum_{j=1}^{n} d_j = 0$, s_n must be zero.

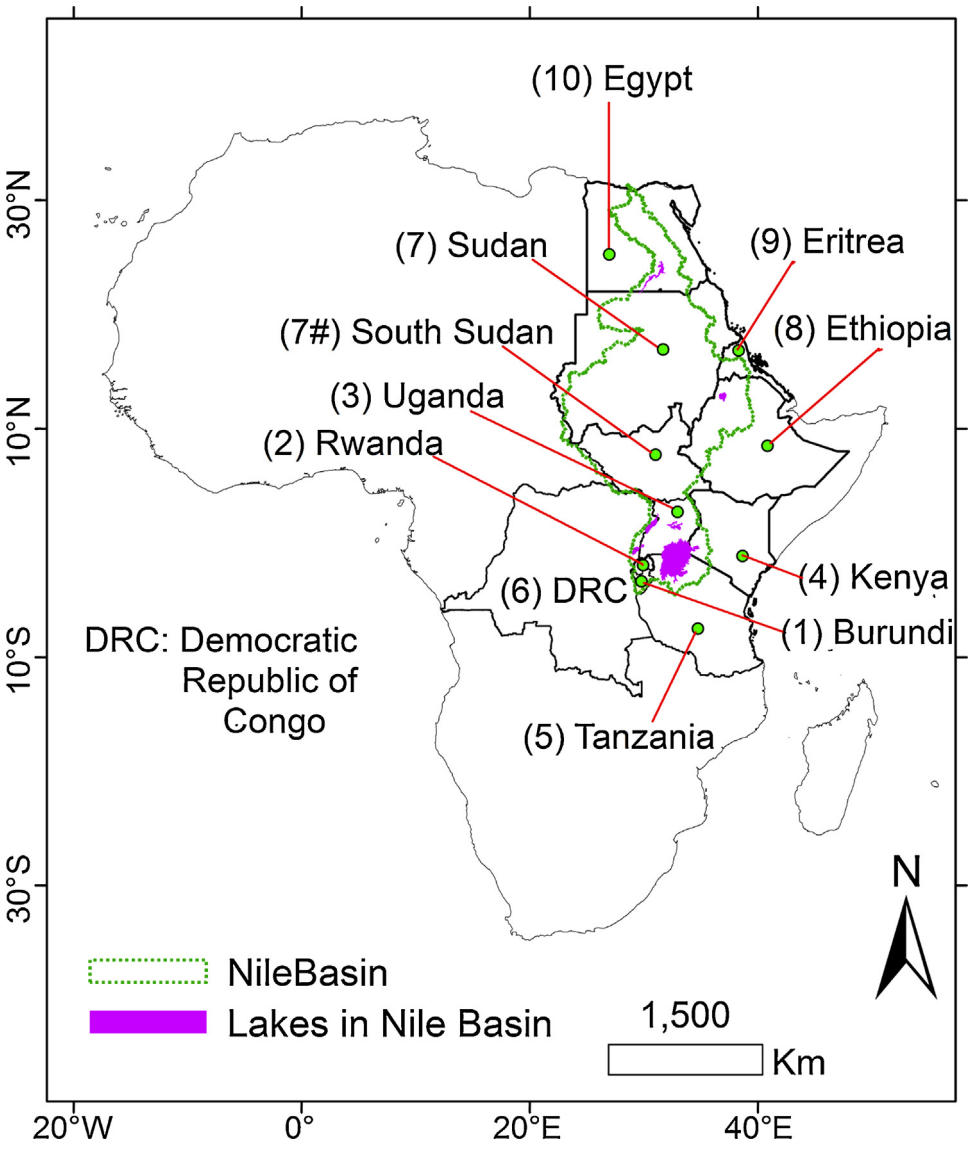

Fig. 1. The NRRCs; the number in () denotes the country ID in this paper.

3.1.1. Graphical CRD analyses of changes

To identify changes in the series over unknown time periods, the CRD plot (i.e. s_i versus the time of the data points) can be used. In the CRD plot as illustrated in Fig. 3, the $s_i = 0$ line is taken as the reference. Positive or negative values of s_i are considered to characterize sub-trends in the series. The portion of the curve above/below the reference as shown by the upward/downward arrow in Fig. 3 indicates a positive/negative sub-trend. More information on how to use the CRD plot for the identification of other forms of changes in the series can be obtained from Appendix A.1. It is required that the significance of the sub-trends visualized from the CRD plot be determined using the statistical means as will be presented in Section 3.1.2.

The uncertainty bounds as illustrated Fig. 3 on the observed changes in the CRD are constructed by employing the technique of resampling and percentile confidence interval in a combined way. The details on the systematic steps for the uncertainty quantification are presented in Appendix A.2.

3.1.2. Statistical analyses of trends

For the conclusiveness of the significance of the trend visualized from the CRD plot in Section 3.1.1, the CRD statistic T is computed using (Onyutha, 2016a):

$$T = \frac{6}{(n^3 - n)} \sum_{i=1}^{n-1} s_i = \frac{6}{(n^3 - n)} \sum_{i=1}^{n-1} \sum_{j=1}^{i} \left\{ 2u_j - \left(n - w_j \right) \right\} \tag{3}$$

The distribution of T is approximately normal (see Appendix A.3) with the mean of zero and variance given in terms of the expression $(1 + n + n^2 + n^3 + \ldots + n^{k-1})/n^k$ where k is the number of series terms. If V_G and V_0 denote the variance of T for data with and without ties respectively, and assuming the contributions from terms higher than 4 (i.e. for $k \geq 5$) are negligible, the distribution of T is characterized by:

$$V_0 = \sum_{k=1}^{4} \frac{1}{n^k} = \frac{1}{n^4} \left(1 + n + n^2 + n^3 \right) \tag{4}$$

$$V_G = V_0 \times \left(1 - \frac{10}{17} y^2 - \frac{7}{17} y \right) \tag{5}$$

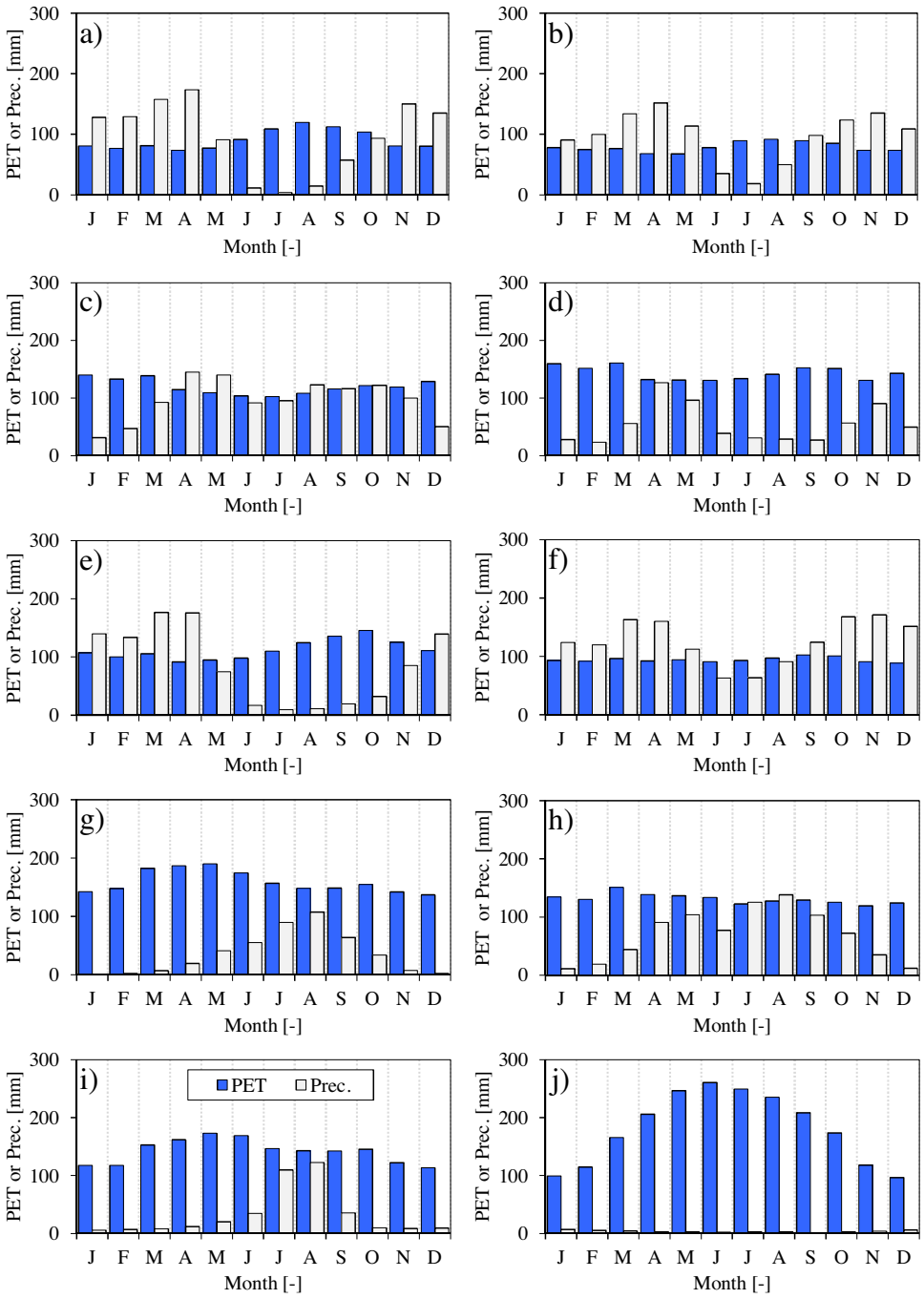

Fig. 2. Mean of long-term monthly PET and precipitation (Prec.) of: (a) Burundi, (b) Rwanda, (c) Uganda, (d) Kenya, (e) Tanzania, (f) DRC, (g) Sudan, (h) Ethiopia, (i) Eritrea, and (j) Egypt. All the charts share the same legend as in (i).

where y (Eq. 6) is the measure of ties in the data,

$$y = \frac{1}{n^2 - n}\left(\sum_{i=1}^{n} w_i - n\right) \tag{6}$$

and w_i is as defined in Eq. (1).

The standardized CRD test statistic Z_{CRD} which follows the standard normal distribution with mean (variance) of zero (one) is given by:

$$Z_{CRD} = \frac{T}{\sqrt{V_G^{\#}}} \tag{7}$$

where $V_G^{\#}$ is the V_G corrected for the influence of autocorrelation. For the steps to obtain $V_G^{\#}$ from V_G the reader is referred to Appendix A.4. A positive (negative) value of T indicates an upward (downward) monotonic trend. The null hypothesis H_0 (no trend), at the significance level α%, is accepted if the $|Z_{CRD}|$ is less than the absolute value of the standard normal variate $Z\alpha_{/2}$; otherwise H_0 is rejected.

Whereas T gives the trend direction, the magnitude of the trend can be obtained in terms of its slope m given by (Sen, 1968; Theil, 1950):

$$m = Median\left(\frac{x_j - x_i}{j - i}\right), \forall i < j \tag{8}$$

where x_j and x_i are the j^{th} and i^{th} observations, respectively.

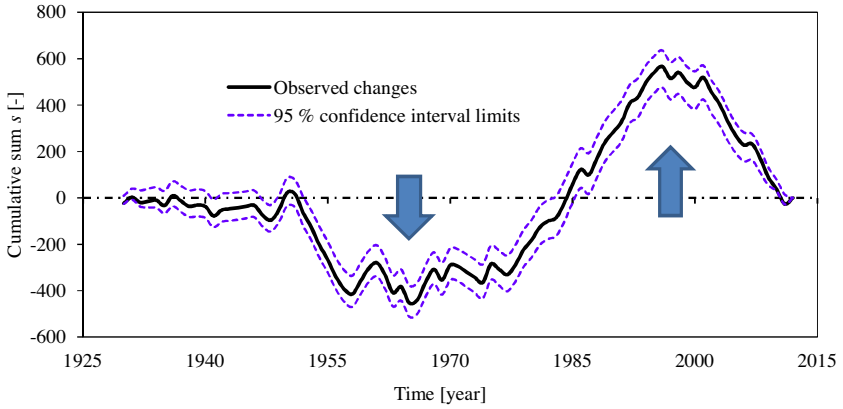

Fig. 3. Observed changes and uncertainty bounds in the CRD plot for JJAS seasonal PET in Kenya.

To construct uncertainty bounds on the trend magnitude and to test the significance of the trend slopes, the EES technique was employed (see Appendices A.5 and A.6 for the details of the procedure used).

3.1.3. Analyses of variability using the nonparametric anomaly indicator method (NAIM)

The two variability computation methods including the autocorrelation spectral analysis and empirical orthogonal functions mentioned in Section 1 normally tend to be applied directly to the original series. This makes them susceptible to the influence of possible outliers in the data if present. Another way to assess variability, as adopted in this study, is to perform temporal convolution of the given series. Convolution or aggregation removes short-term fluctuations from the series and permits the study of the general or summarized and representative behavior of the data (WMO, 2008). The Nonparametric Anomaly Indicator Method NAIM (Onyutha, 2016b,c) was recently proposed to implement the temporal convolution in a way that circumvents the influence of possible outliers in the data while also ensuring that the variability analyses results are not affected by the non-normally distributed data which frequently occur in hydro-meteorology. Eventually, the NAIM was applied to separate the clusters of the PET above or below the long-term average (or reference) using the following steps:

i) select a block length (B_L) based on a sensitivity analysis while ensuring the periods of high or low anomalies are as nearly independent as possible. In this study, to capture the decadal oscillations if any, sensitivity analysis was done using B_L in the range 2–10 years.
ii) transform each value of d_i from Eq. (1) using $q_i = -1 \times d_i$ for $1 \le i \le n$; this is to make the variation pattern of the rescaled series match that of the given data.
iii) using temporal convolution, the anomaly in the j^{th} time slice (a_j) of the transformed data from Step (ii) is given by Onyutha (2016c):

$$a_j\,(\%) = \frac{100}{(n-1)\,B_L} \sum_{i=j}^{g} q_i \tag{9}$$

where $g = j + (B_L - 1)$ and $1 \le j \le (n + 1 - B_L)$.

Actually, the term $(n-1)$ from Eq. (9) is equal to the possible absolute maximum value of q_i from Step (ii).

- finally, plot the values of a_i from Eq. (9) against the mid-points of the time slices.

For the validity of the anomalies from the NAIM, it is vital to verify the null hypothesis (H_0) that there is no persistence in the temporal climate variation; in other words, the variability in the PET is caused by only natural randomness. The H_0 was verified using the variability bounds in the form of confidence interval (CI) constructed using the nonparametric bootstrapping by Monte Carlo simulations (see Appendix B for the procedure). NAIM was applied to the PET to analyze variability. To seek for the attribution of the changes in PET in terms of the rainfall variation, NAIM was also applied to the rainfall series. The co-occurrences of the NAIM results for the PET and those of rainfall were assessed using correlation analyses.

Fig. 4 illustrates the temporal anomaly pattern for the JJAS seasonal PET in Kenya. The long-term average observed change in the PET is represented by the zero percent anomaly which is taken as the reference. The fluctuations of the anomalies above or below the reference characterize the variability. The up and down arrows indicate periods with the PET above and below the reference, respectively. It is noticeable that the changes in the PET are either underestimated or overestimated for lower than higher time slices. To capture the decadal oscillations if any, $B_L = 10$ years was adopted because it gave a more representative convolution of the series than for other values such as $B_L = 2$, 5, and 7 years. In planning for crop water requirements, the period of 10–15 years may be relevant for the design life of some water supply systems of an irrigation scheme. The variability bounds on the anomalies of $B_L = 10$ years were constructed using 95% CI. The temporal oscillation was characterized by its crests (trough) in the mid 1950s and 2000s (mid 1980s). The oscillation low (high) from the mid 1970s to late 1990s (early 1990s to late 2000s) was significant since the observed change down-crossed (up-crossed) the lower (upper) 95% CI limits.

4. Results

4.1. Variability analysis

Fig. 5 shows, for the purpose of illustration, the variability of the annual PET in the NRRCs. The periods during which significant oscillation highs or lows occurred in both the seasonal and annual PET are summarized in Appendix C. From the early 1930s to around 1980s, the annual PET of countries in the equatorial region (Fig. 5a–f) as well as for Sudan (Fig. 5g) and Egypt (Fig. 5j) were below the mean of the full time (long-term) series. The annual PET of Ethiopia (Fig. 5h) was below the reference in the 1940s and mid 1980s; however, oscillation high was in the early 1950s as well as from the late 1990s through to the mid 2000s. For Eritrea (Fig. 5i), the PET from the early 1930s to late 1960s (early 1970s to mid

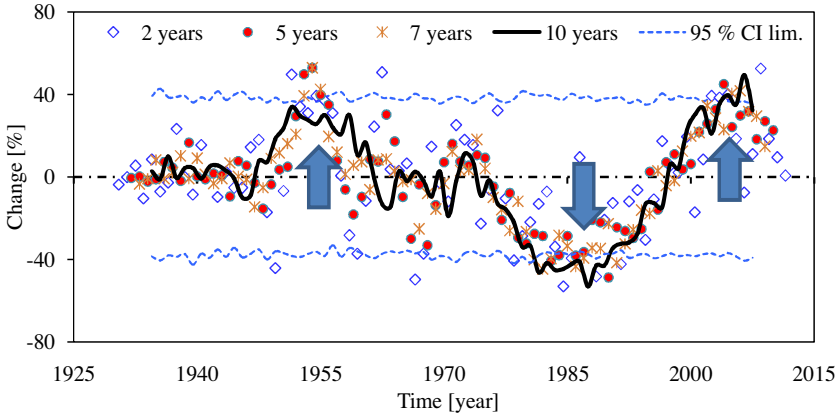

Fig. 4. Results of NAIM applied to the JJAS seasonal PET in Kenya using time slices of 2, 5, 7 and 10 years. "CI lim." denotes confidence interval limits constructed on observed changes using a time slice of 10 years.

Table 1
Statistical trend analysis in the annual and seasonal PET.

Country	U_Z Annual PET	C_F	C_Z	p-val.	Cor.	U_Z MAM seasonal PET	C_F	C_Z	p-val.	Cor.
1	**3.80**	3.38	**2.07**	0.04	−0.13	**4.08**	4.93	1.84	0.07	−0.64
2	**2.74**	2.41	1.76	0.08	−0.35	**2.74**	2.72	1.66	0.10	−0.45
3	**3.75**	6.41	1.48	0.14	0.16	**3.41**	3.44	1.84	0.07	−0.68
4	**1.99**	1.77	1.50	0.13	−0.11	0.92	1.42	0.78	0.44	−0.23
5	**4.01**	3.38	**2.18**	0.03	−0.60	**4.97**	5.24	**2.17**	0.03	−0.85
6	**5.07**	7.14	1.90	0.06	−0.75	**4.25**	3.24	**2.36**	0.02	−0.76
7	**3.51**	6.45	1.38	0.17	−0.37	**2.96**	5.42	1.27	0.20	−0.42
8	1.02	2.34	0.67	0.51	−0.02	1.16	2.72	0.70	0.48	−0.51
9	**3.70**	5.93	1.52	0.13	−0.18	**3.25**	4.38	1.55	0.12	−0.28
10	0.87	4.49	0.41	0.68	−0.28	0.28	1.72	0.21	0.83	−0.40
	JJAS seasonal PET					ONDJF $^{(7-10)}$ or OND $^{(1-6)}$ seasonal PET				
1	**2.04**	1.55	1.64	0.10	−0.33	1.44	1.39	1.22	0.22	−0.26
2	1.11	0.81	1.24	0.22	−0.40	0.72	1.75	0.55	0.58	−0.31
3	**2.97**	3.75	1.53	0.13	−0.55	**2.47**	1.35	**2.13**	0.03	0.14
4	−0.14	2.91	−0.09	1.07	0.08	1.92	1.23	1.73	0.08	−0.23
5	**2.46**	1.42	**2.07**	0.04	−0.63	1.56	1.23	1.41	0.16	−0.43
6	**4.61**	4.71	**2.12**	0.03	−0.30	**3.09**	1.60	**2.44**	0.01	−0.10
7	**3.78**	6.33	1.50	0.13	−0.55	**1.98**	4.26	0.96	0.34	0.13
8	0.96	0.39	1.55	0.12	0.30	1.62	2.17	1.10	0.27	0.43
9	**3.58**	6.71	1.38	0.17	−0.25	**2.70**	5.02	1.20	0.23	0.18
10	**2.92**	6.75	1.13	0.26	0.52	−1.82	2.76	−1.09	1.73	−0.25
	JF seasonal PET					U_Z: Z_{CRD} uncorrected from auto-correlation effect (ACE)				
1	**2.87**	1.61	**2.26**	0.02	−0.14	C_F: correction factor;				
2	**2.24**	1.42	1.88	0.06	−0.57	C_Z: Z_{CRD} corrected from ACE				
3	**3.54**	3.47	1.90	0.06	−0.25	p-val.: p-value of C_Z				
4	**2.58**	2.28	1.71	0.09	−0.16	ONDJF$^{(7-10)}$: for countries labeled 7–10				
5	**3.14**	2.51	**1.98**	0.05	−0.15	OND$^{(1-6)}$: for countries labeled 1–6				
6	**2.81**	1.98	**2.00**	0.05	−0.48	Bold values are trend directions significant at 5% level.				

Underlined values are coefficients of correlation (Cor) (between rainfall and PET) insignificant at 1% level. The critical correlation values are 0.23 and 0.30 at 5% and 1% significance levels respectively.

2000s) were below (above) the reference. It is noticeable that from about the early 1980s to mid 2000s, the PET in most of the NRRCs changed from being below to above the long-term mean or reference. As will be shown shortly later in Table 1, the correlation between the variation in PET and that in rainfall of most NRRCs are significant at the level of 5%.

4.2. Graphical changes in the PET

Fig. 6 shows, for illustration, the annual PET time series of the NRRCs. Though not visibly conclusive for Ethiopia (Fig. 6h), the general increase in the annual PET totals of all the NRRCs (Fig. 6a–j) is noticeable. Fig. 7 shows graphical sub-trends in the annual PET. The periods during which positive and negative sub-trends occurred in both the seasonal and annual PET are summarized in Appendix D. Apart from Egypt (Fig. 7j), the CRD curves of the annual PET of the NRRCs (Fig. 7a–i) were mostly above the reference. This shows that the annual PET was dominated by positive sub-trends. The annual PET in Egypt (Fig. 7j) was characterized by negative (positive) sub-trend from the early 1930s to mid 1960s (the late 1960s to late 2000s). The pattern of the sub-trend in the MAM season (though not shown in Fig. 7) was noted to be comparable with that of the annual PET. This suggested that the changes in the annual PET in Egypt could be influenced by the variations in the MAM seasonal PET. The significance of these visualized trends especially for the long-term period is verified using the statistical CRD results.

4.3. Statistical trend analysis

Table 1 shows results of trends in the PET of the various NRRCs. The null hypothesis H_0 (there is no trend) was accepted at the significance level 5% if the magnitude of Z_{CRD} was less than 1.96;

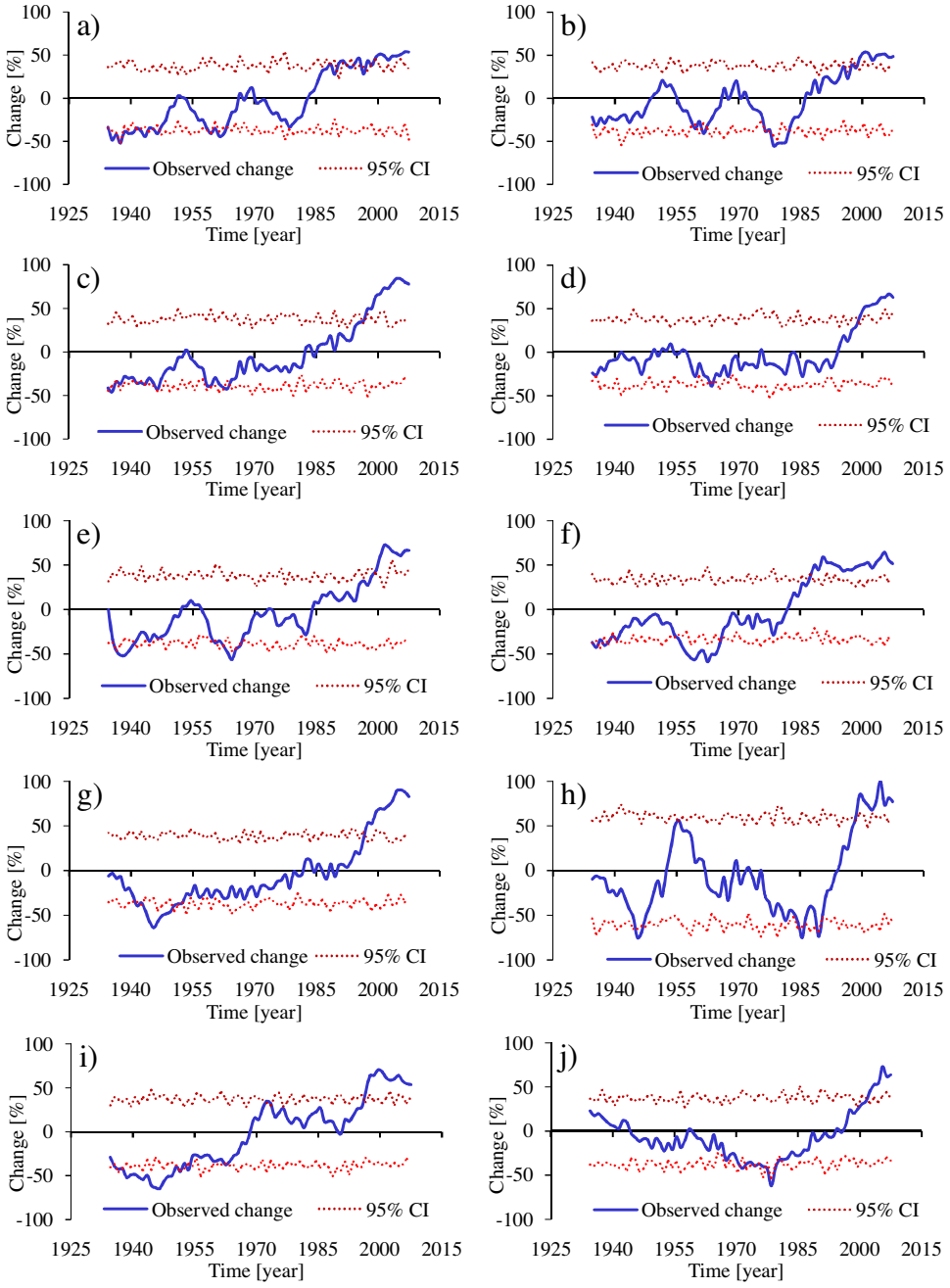

Fig. 5. Results from the NAIM applied to the annual PET in: (a) Burundi, (b) Rwanda, (c) Uganda, (d) Kenya, (e) Tanzania, (f) DRC, (g) Sudan, (h) Ethiopia, (i) Eritrea, and (j) Egypt. In the legend of each chart, 'CI' stands for confidence interval.

otherwise, H_0 was rejected. Using U_Z i.e. the Z_{CRD} uncorrected from the autocorrelation influence, the H_0 was rejected in both the annual and seasonal PET of most NRRCs. This is because the presence of the positive autocorrelation inflates the sampling variance of T which in turn increases the type I error (see Appendix A.4). Thus, it is vital to eliminate the autocorrelation effect in trend results. Eventually, based on the C_Z i.e. Z_{CRD} after applying the correction factor (C_F), trends in the annual PET as well as the series of the MAM and JJAS seasons were significant at 5% level in 2 out of 10 (20%) of the NRRCs. Increasing trends significant at 5% level were also found in the OND seasonal PET of 33% of the six equatorial countries. The trends in the PET of Sudan, Ethiopia, Eritrea and Egypt were insignificant at 5% level.

Trend directions in both annual and seasonal PETs were mainly positive. Some possible factors which can lead to such positive trend direction in the PET include decrease in rainfall, increase in temperature, etc. For both seasonal and annual time scales, the coefficients of correlation between the variation in PET and that in rainfall are also shown in the columns labeled "Cor" in Table 1. It is evident that for most of the NRRCs, the temporal changes in PET especially during rainy seasons can significantly (at 5% level) be explained by the variation in rainfall (Table 1). It is also noticeable that the magnitudes of the correlation tend to vary from one country to another. This could be due to the spatial dissimilarity in microclimate (micro-scale features) or regional features such as water bodies, topography, or transition in land cover and/or use, etc which can influence the variation of rainfall or PET to varying extents. Another cause (though not investigated in this study) of the persistent increase in the atmospheric evaporative demand is the increase in temperature. For developing countries like some

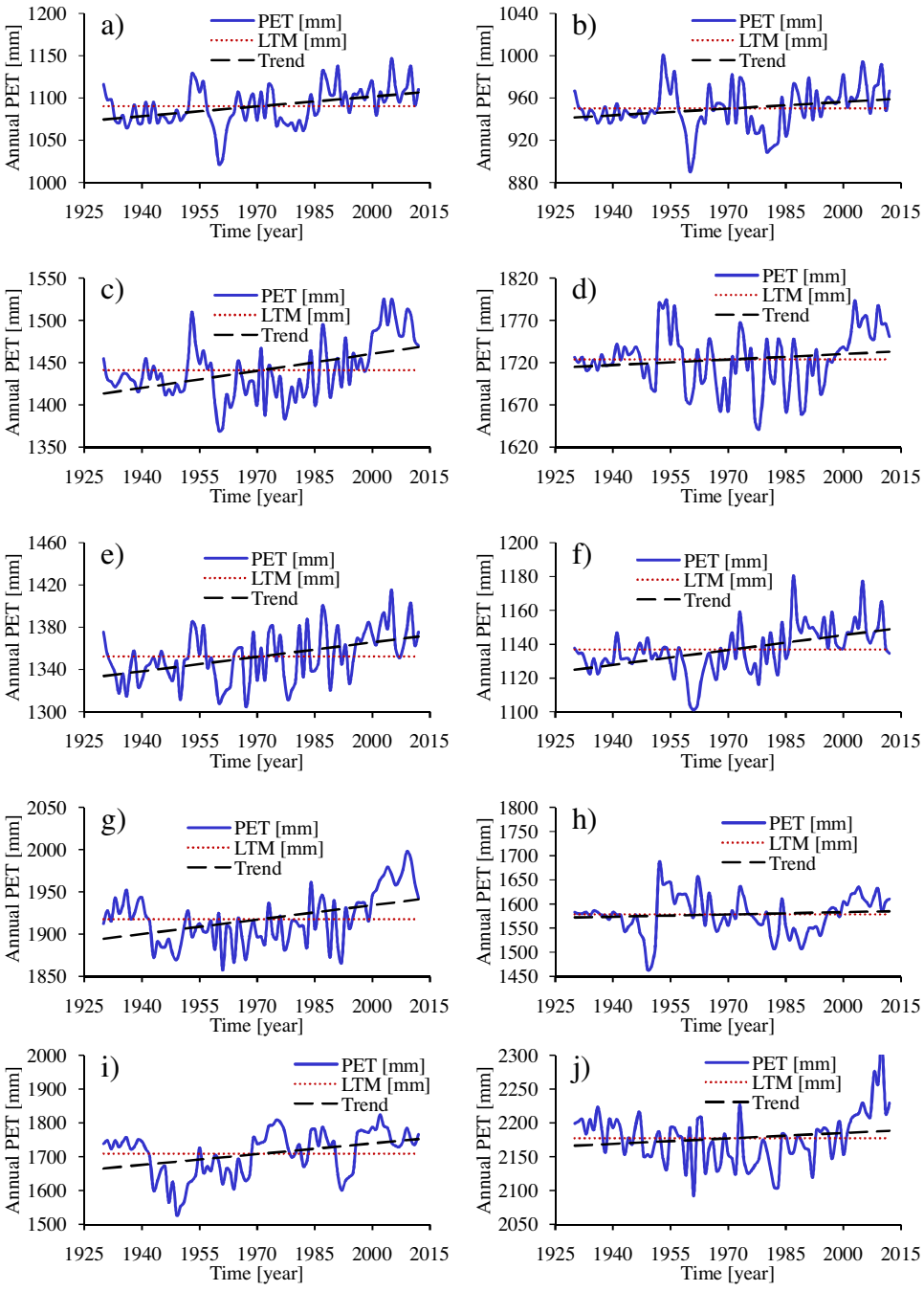

Fig. 6. Linear trends for the annual PET in: (a) Burundi, (b) Rwanda, (c) Uganda, (d) Kenya, (e) Tanzania, (f) DRC, (g) Sudan, (h) Ethiopia, (i) Eritrea, and (j) Egypt. In the legend, "LTM" stands for long-term mean of the PET.

of the NRRCs characterized by high population growth and widespread poverty, such positive trend directions in the PET as shown in Table 1 can lead to decline in soil moisture and negatively affect crop production thereby potentially aggravating the poor condition of majority of the people that utterly tend to depend on agriculture to support their livelihoods.

The magnitudes of the trends in the annual and seasonal PET are shown in Table 2. The slopes of the trends of both annual and seasonal PET were generally positive. This is consistent with the graphical trend results visualized from the CRD plots (Fig. 7). The non-zero magnitude of the increase in the PET over the period 1930–2012 was found significant at the level of 5% in the series of the MAM and OND seasons of Kenya and DRC respectively. The magnitude of the decrease in ONDJF seasonal PET of Egypt was also significant at the level of 5%. Based on the results from Table 1 and Table 2, and considering the selected 5% level of significance, it is noticeable that some countries which exhibited significant trends in their PET series instead showed insignificant magnitude of the increase or decrease in the PET. This demonstrates that for a given series, trend direction can be statistically significant while the trend magnitude or slope is insignificant. Therefore, it is important to question the evidence of H_0 (no trend in the given series) based on the significance of trend slope or magnitude of the increase or decrease in the variable. Such further questioning is vital to support inferential decisions in trend analyses, given that trend direction can be significant for a very small magnitude of change

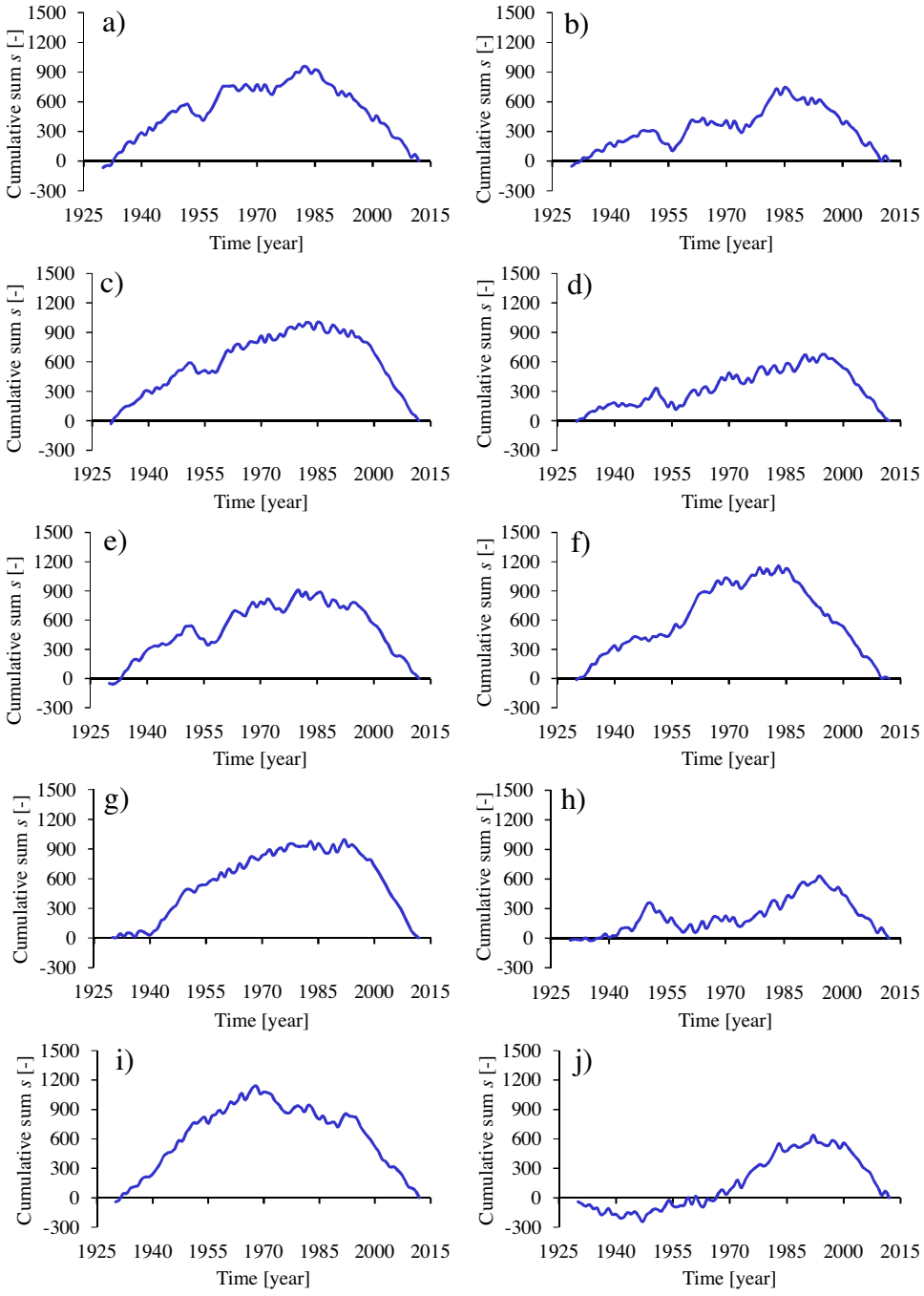

Fig. 7. CRD plots for the annual PET in: (a) Burundi, (b) Rwanda, (c) Uganda, (d) Kenya, (e) Tanzania, (f) DRC, (g) Sudan, (h) Ethiopia, (i) Eritrea, and (j) Egypt.

which may be unimportant in practice. On the contrary, for instance due to noise in the data, the test result may be insignificant for a change whose magnitude cannot be ignored in hydro- or agro-meteorology.

5. Conclusion

This paper has assessed changes in the PET using statistics based on the nonparametric rescaling in terms of the difference between the exceedance and non-exceedance counts of data points. Variability was investigated using the Nonparametric Anomaly Indicator Method (NAIM). The Cumulative Rank Difference (CRD) test was used to detect trends both graphically and statistically. The slopes of the trends were computed based on the method of Sen (1968) and Theil (1950). Sampling uncertainty on the trend magnitude was quantified by employing the Exclude-one and Estimate Slope (EES) technique.

The PET totals from 1930 to around 1970 were generally below the mean of the long-term data. From around 1980 to early 2000s, the PET totals at both annual and seasonal time scales in most of the NRRCs changed from being below to above the reference or the mean of the long-term series. This change in PET totals generally influenced the slope of the long-term trends (though not all significant at 5% level) in the NRRCs over the period 1930–2012 to be positive. For both seasonal and annual time scales, increasing trends in the PET of Sudan, Ethiopia, Eritrea and Egypt were

Table 2
Slope of the trend in annual and seasonal PET.

Country	Annual PET			MAM seasonal PET			JJAS seasonal PET		
	m	L_L	U_L	m	L_L	U_L	m	L_L	U_L
1	0.380	0.367	0.381	0.121	0.120	0.124	0.095	0.090	0.098
2	0.217	0.210	0.221	0.052	0.047	0.053	0.000	0.000	0.000
3	0.632	0.615	0.639	0.170	0.167	0.173	0.179	0.178	0.186
4	0.295	0.284	0.304	**0.049**	0.036	0.048	0.000	0.000	0.000
5	0.481	0.472	0.486	0.170	0.170	0.174	0.085	0.082	0.087
6	0.257	0.254	0.260	0.079	0.078	0.081	0.069	0.069	0.072
7	0.580	0.574	0.595	0.133	0.131	0.138	0.235	0.226	0.235
8	0.098	0.078	0.105	0.000	0.000	0.000	0.000	0.000	0.000
9	0.965	0.942	0.987	0.307	0.302	0.315	0.361	0.356	0.371
10	0.142	0.126	0.153	0.000	0.000	0.000	0.247	0.237	0.253

	ONDJF seasonal PET			OND seasonal PET			JF seasonal PET		
1				0.000	0.000	0.000	0.065	0.064	0.068
2				0.000	0.000	0.000	0.052	0.047	0.053
3				0.130	0.125	0.133	0.132	0.129	0.134
4				0.102	0.099	0.108	0.085	0.083	0.088
5				0.073	0.068	0.077	0.099	0.098	0.102
6				**0.046**	0.033	0.043	0.000	0.000	0.000
7	0.132	0.126	0.137	m: trend slope [mm/year]					
8	0.101	0.100	0.109	L_L and U_L: are respectively the lower and upper 95% confidence interval limits constructed on m.					
9	0.297	0.291	0.312						
10	−0.106	−0.110	−0.101						

Magnitudes of the increase or decrease in the PET significant at 5% level are shown in bold.

insignificant at 5% level. However, for the equatorial region, annual PET exhibited increasing trend directions significant at 5% level in 2 of the 6 countries. Again, positive trend directions significant at 5% level in 2 of the 6 countries were found in the MAM, JJAS and OND seasonal PET. For the JF seasonal PET, positive trend directions significant at 5% level was found in 50% of the 6 countries. Among the countries in the northern part of the Nile Basin, the magnitude of the decrease in ONDJF seasonal PET of Egypt was significant at the level of 5%. For the equatorial region, the magnitude of the increase in the PET was found significant at the level of 5% in the MAM and OND seasonal series of Kenya and DRC respectively.

It was found that the changes in PET especially during rainy seasons of the NRRCs can be significantly (at the level of 5%) explained by the variation in the rainfall. However, based on the temporal patterns of PET variability as assessed in this study, it is recommended that other causes of the PET variability apart from rainfall variation be investigated. Possible driving forces of the PET variability might also come from the variation of other meteorological variables e.g. wind speed, relative humidity, etc. However, due to the possible spatial dissimilarity in the microclimate (micro-scale features) across the various regions of the study area, the variation of hydro-meteorological variables (e.g. PET, rainfall, etc) can also possibly be influenced by regional features such as water bodies, topography, or transition in land cover and/or use. To investigate the influence such regional features on PET variability (though not done in this study), regional numeric modeling capable of reproducing the region's climate would be required. Based on known possible drivers of the PET variation, an insight into the substantial impact of the climate variability on water resources and agricultural management practices can be obtained. This may be valuable especially in the prediction of an upcoming period of decrease or increase in the seasonal and annual PET and hence the assessment of crop water requirements.

To implement the CRD trend test and/or perform variability analyses using the NAIM, the author has made an Excel-based VBA-coded tool named "CRD-NAIM" freely available to the public or interested readers to download online from https://sites.google.com/site/conyutha/tools-to-download.

Acknowledgement

The data series used in this study were obtained from the British Atmospheric Data Centre (BADC) of the Natural Environment Research Council (NERC).

Appendix A. Further information on the CRD method

A.1 Some forms of changes in the CRD plot

For the possible maximum monotonic trend, the CRD curve is described by a quadratic polynomial $s_i = (Hi^2 + Gi + U)$. For positive (negative) trend, $H = -1(1)$ and $G = n(-n)$; however, U is zero for a large n. In other words the possible maximum increasing or decreasing trend is described by $s_i = (ni - i^2)$ or $s_i = (i^2 - ni)$, respectively. In case the trend is not at its maximum magnitude but positive/negative in direction, most part (if not the whole) of the CRD curve falls above/below the reference (See cases (b) and (2), (c) and (3) of Fig. A1). When the series has no trend, the CRD curve crosses the $s_i = 0$ line (reference) a number of times; moreover, there may be no clear area over large time period between the curve and the $s_i = 0$ line (See cases (f) and (6) of Fig. A1). If the series has an increasing (decreasing) trend in the first (second) half, for example, two curves are formed over the two halves of the CRD plot. The first (second) curve is formed on the first (second) half of the period but above (below) the reference (See cases (a) and (1) of Fig. A1). A series may have one half characterized by an increase/decrease while the other half has no trend. In such a case, the CRD will be above/below the reference; however, the curve for the section with no trend will tend to be linear while the part of the series with an increase/decrease will have its scatter points in the form of a curve (which may be incomplete i.e. with its second end not close to the $s_i = 0$ line) (See cases (g) and (7), (h) and (8) of Fig. A1). For a step jump in mean of the series, a number of cases may exist. Firstly, if there is no trend in both parts of the sub-series before and after the step jump, two lines intersect at a point (call it the vertex). This vertex is above/below the reference for a step upward/downward jump. This means the slope of the first line is positive/negative while that for the second one is negative/positive for an upward/downward jump (See cases (d) and (4),

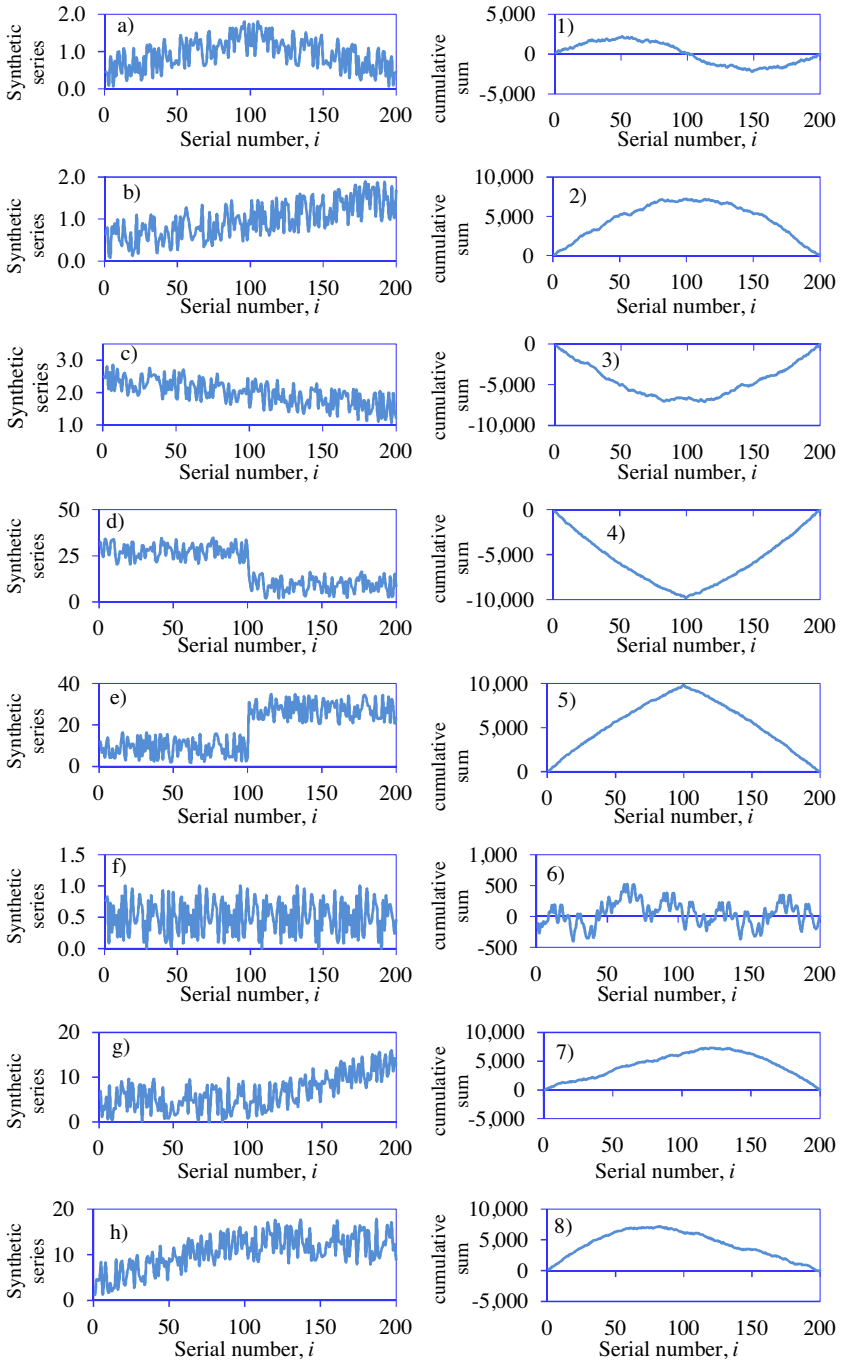

Fig. A1. The plots for (a–h) synthetic series of $n = 200$, and 1)–8) the cumulative effects of the temporal variations for the corresponding series.

(e) and (5) of Fig. A1). Secondly, if the sub-series before and after the step jump all have increasing/decreasing trend, two curves are formed above/below the $s = 0$ line.

i) A.2 Uncertainty quantification in the CRD plot

To construct uncertainty bounds in the form of confidence interval at a selected significance level α% (taken as 5% in this study) on the observed changes in the CRD plot, the following steps are taken:

i) apply Eq. (2) to the original or given series;
ii) select the i^{th} data point of the original series from Step (i);
iii) one at a time, replace the selected data point from Step (ii) by other values from the sample;
iv) apply Eq. (2) to each of the new series from Step (iii); this will yield $(n-1)$ sets of the s_i values;
v) from each set, extract the i^{th} value of s_i;
vi) rank the extracted $(n-1)$ values of s_i from the highest to the lowest;
vii) construct the upper and lower $(100-\alpha)$% confidence interval (CI) limits for the i^{th} data point from Step (ii) using the $[0.005 \times \alpha\% \times (n-1)]^{th}$ and $[\{1-(0.005 \times \alpha\%)\} \times (n-1)]^{th}$ ranked values respectively;
viii) go to the next or $(i+1)^{th}$ data point and repeat steps (ii) to (vii); and

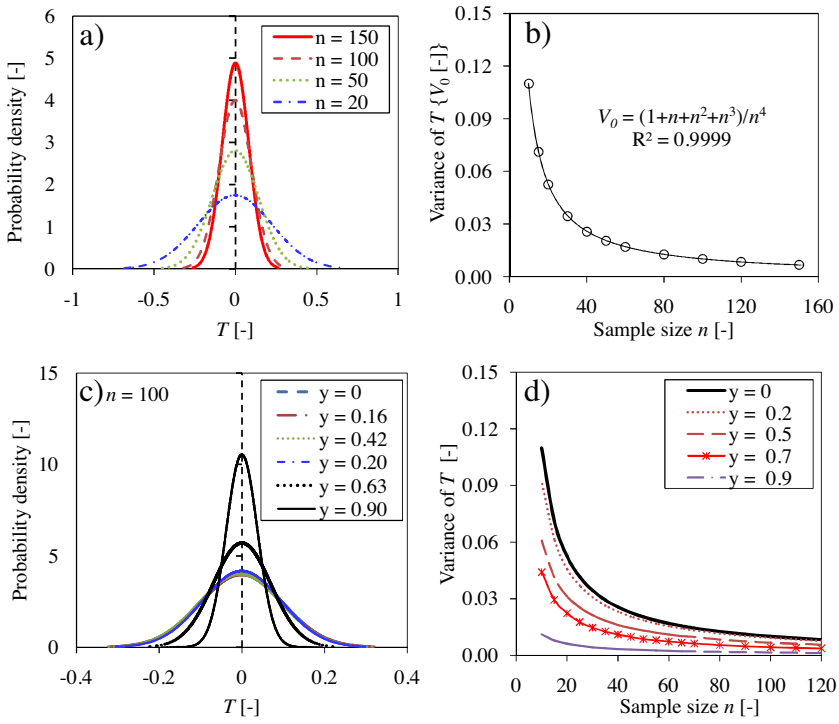

Fig. A2. (a, c) Distribution of T, and (b, d) variance of T versus sample size n.

ix) repeat Step (viii) till the CI limits on all the n values of s_i from step (i) are constructed.

A.3 Distribution of the CRD test statistic T

To obtain Fig. A2, for each selected sample size n in the range 10–150, two million synthetic series were generated. For each dataset, T was computed using Eq. (3). For each selected n, the distribution of T was assessed. The mean of the distribution of T is approximately normal with the mean equal to zero (Fig. A2 a and c). Based on a cursory look at the variation of the variance of T with n (Fig. A2 b), the validity of Eq. (4) to fit through the scatter points comes almost intuitively. By increasing various measures y of random ties in the synthetic series, the distribution of T becomes more peaked or in other words the variance gets more deflated (Fig. A2 c). Eventually, the higher the value of y, the lower the position that its curve occupies (Fig. A2 d). The variance deflation due to ties can be described by a quadratic polynomial function in terms of y. To derive this equation, three conditions are required two of which are known. Firstly, when $y = 1$ (i.e. completely no trend case), the variance of T is zero. Secondly, when $y = 0$ (i.e. no ties), V_0 from Eq. (4) is valid and gives the third term of the quadratic equation, also known as the constant or free term. Although practically y varies from zero to one, the validity of the polynomial function outside this range can be assumed to obtain the third unknown point. Thus, when $y = -17/10$, the variance of T is again zero. Based on these three conditions, the leading and the linear coefficients can be obtained accordingly as expressed in Eq. (5).

i) A.4 CRD test statistic variance correction

According to Matalas and Langbein (1962), there is less information about the mean of a time series with positive serial correlation than a random dataset i.e. the effective sample size of the independent sample becomes less than the actual sample size. This is because the variance of the mean estimated from a positively autocorrelated series is inflated. Inflation of the test statistic variance increases the type I error (significance α) i.e. the probability of rejecting the null hypothesis H_0 (there is no trend in the data), when it is true. On the other hand, an anti-autocorrelation deflates the test statistic variance thereby leading to an increase in the type II error (i.e. the probability of accepting the H_0 while it is false). According to Bayley and Hammersley (1946), to correct the affected variance of the mean of autocorrelated data, an effective number of observations can be used. In this same line, the following empirical variance correction steps can be used.

i) The V_G for the given data X_i is computed using Eq. (5).
ii) The linear trend is estimated using Eq. (8).
iii) The detrended series Y_i is obtained as:

$$Y_i = X_i - mi \tag{A1}$$

If m is not removed, the estimation of the magnitude of the serial correlation from the data is contaminated, and this in turn reduces the accuracy of the estimated effective sample size (Yue and Wang, 2004).

- Values of the serial correlation r_k of the new series Y_i are computed using (Salas et al., 1980):

$$r_k = \frac{\frac{1}{(n-k)}\sum_{i=1}^{n-k}[Y_i - E(Y_i)]\,[Y_{i+k} - E(Y_i)]}{\frac{1}{n}\sum_{i=1}^{n}[Y_i - E(Y_i)]^{-2}} \tag{A2}$$

where $E(Y_i)$is the mean of the Y_i series.

The confidence interval limits (L_{CI}) on the r_k based on the formula from Anderson (1941) and Salas et al. (1980) are calculated using Eq. (A3). This should be done using the significance level α% as that chosen for conducting the CRD test. Determine which values of the r_k are significant (call them r_k^{α}) at α%. Only the r_k^{α} values are used so as to circumvent the adverse effect on the estimated vari-

ance which might result from the use of all the r_k values (Hamed and Rao, 1998).

$$L_{CI} = \frac{-1 \pm Z_{\alpha/2}\sqrt{n-k-1}}{n-k} \quad (A3)$$

where $Z\alpha_{/2}$ is the standard normal variate at the significance level α%.

Based on Eq. (A3), it is noticeable that when $k = n-1$, both limits of the confidence interval unrealistically get equal to a single value of -1. To avoid this, k should be set to vary from $k = 1$ up to $n-2$ in Eqs. (A2) and (A3).

- The variance correction factor C_F to account for the autocorrelation is computed using:

$$C_F = |1 + \frac{2}{n\left(n^2-3\right)} \times \sum_{k=1}^{n-2}(n-k)^3 r_k^{\alpha}| \quad (A4)$$

- Finally, V_G from Step (i) is corrected from the influence of autocorrelation to obtain $V_G^{\#}$ using:

$$V_G^{\#} = C_F \times V_G \quad (A5)$$

The standardized CRD test statistic Z_{CRD} which follows the standard normal distribution with mean (variance) of zero (one) is computed using Eq. (7). The p-value (probability value, p) for the Z_{CRD} is computed as the cumulative density function (F) (Eq. (A6)) of the normal distribution based on the standard case with the mean $\mu = 0$ and standard deviation $\sigma = 1$.

$$p = F(Z_{CRD}|\mu,\sigma) = \frac{1}{2} - \frac{1}{\sigma\sqrt{2\pi}}\int_0^{|Z_{CRD}|} \exp\left(-\frac{1}{2}\left\{\frac{t-\mu}{\sigma}\right\}^2\right) dt \quad (A6)$$

To check on the effectiveness of the variance correction (VC) procedures, 2000 Monte Carlo simulations based on first-order (Markov) autoregressive AR(1) stochastic process C_j with mean $\mu_C = 1.0$ and standard deviation $S_C = 1.0$ were made using Eq. (A7) for $n = 40$ and 100, linear trend slope $m = 0.0002$ and lag-1 serial correlation coefficient $r_1 = -0.9(0.3)0.9$. Type I error R_{ej} (i.e. rate of rejection of the null hypothesis H_0 of no trend) based on Eq. (A8) was computed before and after applying correction to the test statistic variance.

$$C_j = \mu_C + r_1\left(C_{j-1} - \mu_C\right) + \varepsilon_j + mj \quad (A7)$$

where ε_j is the white-noise process with mean $\mu_\varepsilon = 0$ and standard deviation $\sigma_\varepsilon = S_C \times \left(1 - r_1^2\right)^{0.5}$

$$R_{ej} = N_{ej}/2000 \quad (A8)$$

where N_{ej} is the number of simulations for which the H_0 was rejected.

Fig. B1 shows the rejection rate of the trend test before and after the application of VC. It is noticeable that the rejection rates are higher for the series with than without VC. For $r_1 > 0$, as the serial correlation increases, the rejection rate increases as well. However, the opposite is noted for $r_1 < 0$, i.e. the rejection rate reduces as the absolute value of r_1 increases. This is because positive (negative) autocorrelation in the data inflates (deflates) the variance of the trend statistic. As the positive r_1 is increased, the distribution of Z_{CRD} gets characterized by an increase in the spread of its tails (Fig. B1 c and d). Normally, for the case where there is no trend in the series ($m = 0$), the mean of the distribution Z_{CRD} is expected to be zero. It is expected that after application of the VC, the rejection rate should reduce to the nominal significance level $\alpha = 0.05$ which was used to perform the CRD trend test on the simulation experiments. This is evident in Fig. B1 a and b. Moreover, effective elimination of the effect of autocorrelation on trend would make the distributions of Z_{CRD} for the different values of r_1 to exhibit comparable variance or amount of spread in the tails. This, again is demonstrated in Fig. B1 e and f.

i) A.5 Uncertainty quantification on the non-zero trend slope

To construct uncertainty bounds in terms of the confidence intervals on the non-zero trend magnitude, the method herein termed as Exclude-one and Estimate Slope (EES) was employed using the following steps:

i applying Eq. (8) to the original or given series of size n to compute m;
ii excluding or leaving out the i^{th} data point from the series from Step (i);
iii computing m using the $(n-1)$ data points from Step (ii);
iv repeating Steps (ii) to (iii) n times to obtain n number of m values;
v quantifying the uncertainty on $\bar{m}$ i.e. the mean of n values of m in the form of $(100-\alpha)$% confidence interval (CI) based on t-distribution and the standard error of the mean using:

$$(100-\alpha)\%CI = \bar{m} \pm t_{\alpha/2,(n-1)} \times \sqrt{\frac{1}{n(n-1)}\sum_{i=1}^{n}(m_i - \bar{m})^2} \quad (A9)$$

where m_i is the slope estimate from the i^{th} subsample.

A.6 Significance of the non-zero slope of linear trend

If m from Step (i) of the EES from Section A.5 falls outside the $(100-\alpha)$% CI limits from Eq. (A9), it means that the increase or decrease in the magnitude of the trend is significant at the level of α% i.e. the non-zero magnitude of m is probably not due to natural randomness in the series. It is recommended that α% used in the EES should be similar to that adopted for testing the significance of the trend directions.

Appendix B. Test of significance for the NAIM results

For the validity of the anomalies from the NAIM, it is vital to verify the null hypothesis (H_0) that there is no persistence in the temporal climate variation; in other words, the variability in the variable under consideration (e.g. PET in this study) is caused by only natural randomness. The H_0 can be verified using the non-parametric bootstrapping (Davidson and Hinkley, 1997) by Monte Carlo simulations. Based on N_{MC} as the number of Monte Carlo simulations, the variability bounds in the form of $(100-\alpha)$% CI were constructed as follows:

(1) applying the NAIM to the original series;
(2) randomly shuffling the original full time series;
(3) dividing the series with new temporal sequence into subseries each of length B_L;
(4) applying the NAIM to the shuffled series;
(5) repeating Steps (2)–(4) N_{MC} times to obtain N_{MC} anomaly values for each subseries;
(6) ranking the anomaly values from the highest to the lowest, and
(7) taking the upper and lower limits of the $(100-\alpha)$% CI as the $[0.005 \times \alpha\% \times N_{MC}]^{th}$ and $[\{1-(0.005 \times \alpha\%)\} \times N_{MC}]^{th}$ anomaly values, respectively.

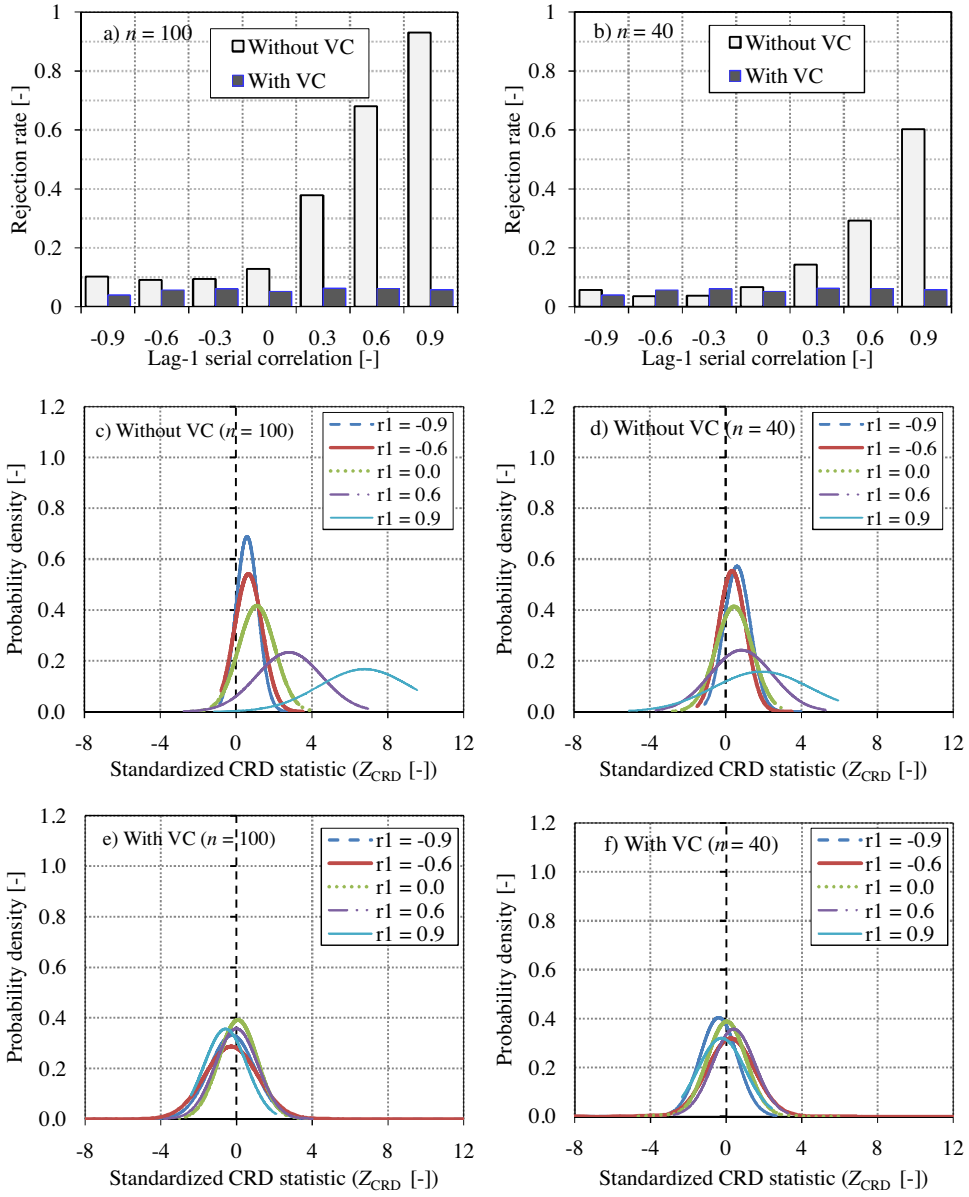

Fig. B1. (a, b) Rejection rate, and probability density of the Z_{CRD} (c, d) without and (e, f) with variance correction.

The H_0 (natural randomness) is accepted/rejected if the anomaly values from Step (1) fall within/outside the CI. In this study, α% and N_{MC} were set to 5% and 1000, respectively.

Appendix C. Significant variability periods in the annual and seasonal PET

Country	Time scale	Oscillation low period	Oscillation high period	Country	Time scale	Oscillation low period(s)	Oscillation high period(s)
Burundi	MAM	1937–1948	1986–1996	DRC	MAM	1956–1962	1988–1997
	JJAS	1974–1980	1997–2004				2001–2008
	OND	1980–1983	1951–1954		JJAS	1956–1964	1985–1994
	JF	1958–1965	2006–2008				1997–2007
	Annual	1935–1947	1985–2008		OND	1962–1966	1988–1995
Rwanda	MAM	1978–1982	2003–2008				2005–2008
	JJAS	1976–1981	2000–2006		JF	1957–1967	2001–2008
	OND	1978–1983	1951–1954		Annual	1955–1965	1988–2008
	JF	1959–1966	2006–2008	Sudan	MAM	1945–1947	2002–2008
	Annual	1976–1982	1997–2008		JJAS	1945–1958	1999–2008
Uganda	MAM	Nil	2002–2008		ONDJF	Nil	2002–2008
	JJAS	1976–1978	1999–2008		Annual	1945–1947	1999–2008
	OND	1961–1966	2001–2008	Ethiopia	MAM	1944–1948	1954–1961
	JF	Nil	2002–2008			1982–1991	2000–2007
	Annual	1934–1936	1999–2008		JJAS	1945–1948	1955–1961
Kenya	MAM	Nil	2004–2008			1981–1990	

	JJAS	1981–1990	2004–2007		ONDJF	1945–1947	2000–2008
	OND	1960–1965	2001–2008		Annual	1945–1947	1999–2008
	JF	Nil	2003–2008	Eritrea	MAM	1945–1949	1997–2006
	Annual	Nil	2000–2008		JJAS	1944–1954	1999–2001
Tanzania	MAM	1935–1939	2000–2008		ONDJF	1943–1949	1997–2008
	JJAS	1935–1938	1999–2002		Annual	1938–1950	1997–2008
	OND	1962–1964	Nil	Egypt	MAM	1965–1973	1934–1939
	JF	Nil	2000–2008		JJAS	Nil	2002–2008
	Annual	1936–1938	1999–2008		ONDJF	1977–1988	Nil
	Annual	1978–1980	2003–2008				

Appendix D. Periods of negative and positive sub-trends in the annual and seasonal PET

Country	Time scale	Periods of negative sub-trends	Periods of positive sub-trends	Country	Time scale	Periods of negative sub-trends	Periods of positive sub-trends
Burundi	MAM	1930–1934	1935–2012	DRC	MAM	2011–2012	1930–2010
	JJAS	1930–1933	1934–2012				
	OND	1930–1933	1934–2012		JJAS	2011–2012	1930–2010
	JF	1930–1934	1935–2012				
	Annual	1930–1932	1933–2012		OND	1930–1933	1934–2009
Rwanda	MAM	1930–1938	1939–2012				
	JJAS	1930–1935 1955–1959	1936–1954 1960–2009		JF	1930–1933	1934–2009
	OND	1953–1967 1971–1977	1940–1952 1978–2012		Annual	1930–1931	1932–2012
	JF	1930–1931	1932–2012	Sudan	MAM	Nil	1930–2012
	Annual	1930–1932	1933–2012		JJAS	1930–1944	1945–2010
Uganda	MAM	1930–1932	1933–2010		ONDJF	1933–1944	1945–2012
	JJAS	1930–1944	1945–2012		Annual	Nil	1930–2012
	OND	1930–1931	1932–2012	Ethiopia	MAM	1938–1939	1930–1937
	JF	Nil	1930–2012				1940–2012
	Annual	1930–1931	1932–2012		JJAS	1931–1942	1943–1959
Kenya	MAM	1954–1976	1930–1953 1977–2012			1960–1979	1980–2012
	JJAS	1930–1984	1985–2008		ONDJF	1930–1931	1932–2012
	OND	1930–1931	1932–2012		Annual	1930–1936	1937–2012
	JF	1930–1931	1932–2012	Eritrea	MAM	1930–1931	1932–2012
	Annual	1930–1931	1932–2012		JJAS	1930–1931	1932–2012
Tanzania	MAM	1930–1931	1932–2012		ONDJF	1930–1931	1932–2012
	JJAS	1930–1932 2004–2012	1933–2003		Annual	1930–1931	1932–2012
	OND	1930–1937	1938–2012	Egypt	MAM	1930–1967	1968–2012
	JF	1930–1931	1932–2012		JJAS	1930–1934	1935–2012
	Annual	1930–1933	1934–2012		ONDJF	1930–1987	1988–2012
					Annual	1930–1966	1967–2012

References

Alemu, H., Senay, G.B., Kaptue, A.T., Kovalskyy, V., 2014. Evapotranspiration variability and its association with vegetation dynamics in the Nile Basin, 2002–2011. Remote Sens. 6, 5885–5908.

Allen, R.G., Jensen, M.E., Wright, J.L., Burman, R.D., 1989. Operational estimates of reference evapotranspiration. Agron. J. 81, 650–662.

Anderson, R.L., 1941. Distribution of the serial correlation coefficients. Ann. Math. Stat. 8, 1–13.

BADC., 2014. CRU year-by-year variation of selected climate variables by country. Available at: http://badc.nerc.ac.uk/view/badc.nerc.ac.uk__ATOM__DE_56531370-2613-11e3-9fca-00163e251233 (retrieved 17.06.14.).

Bashir, M., Tanakamaru, H., Tada, A., 2008. Remote Sensing-based Estimates of Evapotranspiration for Managing Scarce Water Resources in the Gezira Scheme, Sudan. In: Taniguchi, M., Burnett, W.C., Fukushima, Y., Haigh, M., Umezawa, Y. (Eds.). From Headwaters to the Ocean, Hydrological Change and Water Management, Kyoto, Japan, pp. 381–386.

Bayley, G.V., Hammersley, J.M., 1946. The "effective" number of independent observations in an autocorrelated time series. J. R. Stat. Soc. 8, 184–197.

Blackman, R.B., Tukey, J.W., 1959. The Measurement of Power Spectra. Dover Publications, New York.

Camberlin, P., 2009. Nile basin climates. In: Dumont, H.J. (Ed.), The Nile: Origin, Environments, Limnology and Human Use, Monographiae Biologicae, vol. 89. Springer, Dordrecht, pp. 307–333.

Davidson, A.C., Hinkley, D.V., 1997. Bootstrap Methods and Their Application. Cambridge University Press, Cambridge, UK, pp. 582.

FAO., 1997. Irrigation potential in Africa: a basin approach. FAO Land and Water Bull. 4, M-54, ISBN 92-5-103966-6.

Hamed, K.H., Rao, R., 1998. A modified Mann-Kendall trend test for autocorrelated data. J. Hydrol. 204, 182–196.

Harris, I., Jones, P.D., Osborn, T.J., Lister, D.H., 2014. Updated high-resolution grids of monthly climatic observations—the CRU TS3.10 dataset. Int. J. Climatol. 34, 623–642.

IWMI., 2014. East Africa. Available at: http://eastafrica.iwmi.cgiar.org/ (retrieved 01.02.14.).

Kendall, M.G., 1975. Rank Correlation Methods, Fourth ed. Charles Griffin, London.

Kundzewicz, Z.W., Robson, A., 2000. Detecting Trend and Other Changes in Hydrological Data. World Climate Program-Water, WMO/UNESCO, WCDMP-45, WMO/TD 1013, Geneva, pp. 157.

Lehmann, E.L., 1975. Nonparametrics, Statistical Methods Based on Ranks. Holden-Day Inc., Carlifornia.

Mann, H.B., 1945. Nonparametric tests against trend. Econometrica 13 (3), 245–259.

Matalas, N.C., Langbein, W.B., 1962. Information content of the mean. J. Geophys. Res. 67 (9), 3441–3448.

Nicholson, S.E., 1996. A review of climate dynamics and climate variability in Eastern Africa. In: Johnson, T.C., Odada, E.O. (Eds.), The Limnology, Climatology and Paleoclimatology of the East African Lakes. Gordon and Breach, Amsterdam, The Netherlands, pp. 25–56.

Onyutha, C., Tabari, H., Taye, M.T., Nyandwaro, G.N., Willems, P., 2015. Analyses of rainfall trends in the Nile River Basin. J. Hydro Environ. Res., http://dx.doi.org/10.1016/j.jher.2015.09.002 (in press).

Onyutha, C., 2016a. Identification of sub-trends from hydro-meteorological series. Stoch. Environ. Res. Risk Assess. 30, 189–205.

Onyutha, C., 2016b. Variability of seasonal and annual rainfall in the River Nile riparian countries and possible linkages to ocean–atmosphere interactions. Hydrol. Res. 47, 171–184.

Onyutha, C., 2016c. Influence of hydrological model selection on simulation of moderate and extreme flow events: a case study of the Blue Nile Basin. Adv. Meteorol., 1–28, http://dx.doi.org/10.1155/2016/7148326-.

Salas, J.D., Delleur, J.W., Yevjevich, V., Lane, W.L., 1980. Applied Modelling of Hydrologic Time Series. Water Resources Publications, Littleton, Colorado, USA, pp. 484.

Sen, P.K., 1968. Estimates of the regression coefficient based on Kendall's tau. J. Am. Stat. Assoc. 63, 1379–1389.

Sneyers, R., 1990. On the Statistical Analysis of Series of Observations. Tech. Note 143, WMO no. 415, Geneva, Switzerland, pp. 192.

Spearman, C., 1904. The proof and measurement of association between two things. Am. J. Psychol. 15, 72–101.

Theil, H., 1950. A rank-invariant method of linear and polynomial regression analysis. Ned. Akad. Wetench. Ser. A 53, 386–392.

WMO, 1966. Climatic Change. Tech. Note No. 79, WMO, Geneva, Switzerland, pp. 79.
WMO, 2008. Hydrological Data, In: Manual on Low-flow Estimation and Prediction. Operational Hydrology Report No. 50, WMO-No.1029, Geneva Switzerland138.
Yue, S., Wang, C., 2004. The Mann–Kendall test modified by effective sample size to detect trend in serially correlated hydrological series. Water Resour. Manage. 18, 201–218.
Yue, S., Pilon, P., Cavadias, G., 2002. Power of the Mann-Kendall and Spearman's rho tests for detecting monotonic trends in hydrological series. J. Hydrol. 259, 254–271.